

Polarization Variability Arising from Clumps in the Winds of Wolf-Rayet Stars

Q. Li^{1,3*}, J. P. Cassinelli², J. C. Brown³ and R. Ignace⁴

¹ Dept. of Astronomy, Beijing Normal University, Beijing 100875, China

² Dept. of Astronomy, University of Wisconsin-Madison, 53711, USA; cassinelli@astro.wisc.edu

³ Dept. of Physics and Astronomy, University of Glasgow, Glasgow, G12 8QQ, Scotland, UK; john@astro.gla.ac.uk

⁴ Dept. of Physics and Astronomy, Eastern Tennessee State University, USA; ignace@etsu.edu

Abstract The polarimetric and photometric variability of Wolf-Rayet (WR) stars as caused by clumps in the winds, is revisited. In the model which is improved from Li et al. 2000, the radial expansion of the thickness is accounted for, but we retain the dependence on the β velocity law, stellar occultation effects. We again search for parameters that can yield results consistent with observations in regards to the mean polarization \bar{p} , the ratio $\mathcal{R} = \sigma_p/\sigma_{\text{phot}}$ of polarimetric to photometric variability, and the volume filling factor f_V . Clump generation and spatial distribution are randomized by the Monte Carlo method so as to produce clumps which are, in the mean, distributed uniformly in space and have time intervals with a Gaussian distribution. The generated clumps move radially outward with a velocity law determined by a β index, and the angular size of the clumps is assumed to keep fixed. By fitting the observed $\sigma_p/\sigma_{\text{phot}}$ and the volume filling factor f_V , the clump velocity law index β (~ 2) and clump ejection rate \mathcal{N} (~ 1) are inferred, and are found to be well constrained. In addition, the subpeak features on broad emission lines seem to support the clump ejection rate. Meanwhile, the fraction of the total mass loss rate that is contained in the clumps is obtained by fitting the observed polarization. We conclude that this picture for the clump properties produces a valuable diagnostic of WR wind structure.

Key words: Polarization — stars: mass loss — stars: Wolf-Rayet — stars: winds, outflows

1 INTRODUCTION

The intrinsic polarization of hot stars results from the scattering of starlight by electrons in aspherical stellar winds. There is evidence that the asymmetry is not from a fixed structure but rather from stochastic ejection of clumps from the base of hot star winds. This evidence has been accumulating from a variety of spectropolarimetric studies that show that variability appears at a wide range of timescales of days, weeks, and months (Lupie & Nordsieck 1987; Taylor et al. 1991). In the case of Wolf-Rayet stars, detailed observational data on the photometric, polarimetric, and spectral line profile variability have been presented and discussed by numerous authors (e.g., St.-Louis et al. 1987; Drissen et al. 1987; Robert et al. 1989; Drissen et al. 1992; Moffat & Robert 1992; Robert 1992; Lepine et al. 2000). Moffat & Robert (1992) and Lepine & Moffat (1999) have interpreted the Wolf-Rayet observations in terms of a distribution of dense clumps which result from hierarchical turbulence in the stellar winds. Brown et al. (1995) have discussed some of the physical properties of the larger clumps which dominate aspects of the data. Brown (1993) and Brown et al. (1999) conclude that clumps arise either by localized mass loss enhancements at the stellar surface or by the action of radiatively driven shocks sweeping up material on large scales. Brown et al. (2004) have discussed the combining effects of clumping and multiple scattering on the “momentum paradox” of WR star winds.

With the systematic monitoring campaigns for WR stars, Robert et al. (1989) and Robert (1992) find that statistically, WR stars display polarization about 0.1%, and show broad band polarimetric variation ($\sigma_p \approx 0.1\% - 0.02\%$) that is much smaller than the fractional photometric variability (σ_{phot}), the mean ratio being about $\mathcal{R} = \sigma_p/\sigma_{\text{phot}} \approx 0.05$. Richardson et al. (1996) investigate the statistical effect of having

larger numbers of clumps present and conclude that the clumps must be very dense so that their emission ($\propto n^2V$) is large enough to increase σ_{phot} and/or their optical depth is large enough to reduce σ_{p} by multiple scattering. Li et al. (2000) revisited the analysis by carrying out numerical simulations, following clump flow from the star with a β velocity law while accounting for the occultation of clumps behind the stellar disk, but while also retaining the single scattering assumption. They concluded that the clumps follow a large β velocity index, which means that the clumps are accelerating relatively slowly with radius in the wind. They also derived a certain range of clump ejection rate that along with β allows for a fit to the statistical data. Valuable constraints on the WR parameters, such as mass loss rate, can be inferred from the observed mean polarization \bar{p} (about 0.1% level), the polarimetric and photometric variances. These conclusions are supported when considered in conjunction with the number of distinct narrow features that are seen in emission line profiles.

As for the observational evidence on clumping of hot stars in other wavebands, Ignace, Quigley, & Cassinelli (2003) used the observations with the Infrared Space Observatory (ISO) SWS spectrometer to constrain the velocity law and wind clumping, and found that a β -value of the velocity law of the wind is about 2 – 3 and the volume filling factor is up to 40% for WR 136. Marchenko et al. (2006) obtain numerous overdense clumps in the wind of WR 135 with FUSE observations. Chandra high resolution spectral observations of line profiles have shown the clumping wind properties of hot stars (Owocki & Cohen 2006; Oskinova, Hamann, & Feldmeier 2007; Cassinelli et al. 2008).

Recently, Davies et al. (2007) used the clump-ejection model to study the polarimetric variability of hot stars, in particular of luminous blue variables (LBVs), and got the detailed clump parameters through their simulations. One of their conclusions is that many tiny clumps are ejected around hot stars. Of particular interest to us is that Davies et al. (2007) find a flaw in assumptions of Li et al. (2000), in their assumption that both the thickness of a clump is fixed and that the number of electrons in a clump is constant. These results from Davies et al. (2007) motivate us to update the model of Li et al. (2000). It is our goal to understand the general nature of the Wolf-Rayet stars, using a picture for the ejection of clumps into the wind. Here we allow for the thickness of a clump to vary with the wind flow. We find that the main conclusions in Li et al. (2000) still hold, and that the present model leads to well constraints on the parameters, such as β and \mathcal{N} .

The basic model scenario is presented in Section 2, where the basic formulation concerned with the polarization and scattering light of both a single clump and ensemble of clumps are taken into account for various β and \mathcal{N} . In Section 3, the model results are presented and discussed, and in Section 4 general conclusions are presented.

2 CLUMPING MODEL

2.1 Basic Formulation of Polarization for A Single Clump

We assume that the polarimetric and photometric variability of a WR star is due to localized mass ejections at the stellar surface, over which the clumps are generated at random positions, and at random time intervals with a normal distribution of mean value Δt . The clumps are then taken to move radially outward with a velocity law, thus the thickness Δr of the clump should simultaneously expand along the radial wind flows, while the solid angle $\Delta\Omega$ is assumed constant (The geometry of a single outflowing clump is shown in Fig. 1). The electron density then decreases as $r^{-2}v^{-1}(r)$. The clumps thus have axisymmetric shapes and, on the assumption that they are not optically thick in the continuum, the results of Brown & Mclean (1977) can be used to find the polarization of a single clump as:

$$p = \tau_{\text{opt}} (1 - 3\gamma) \sin^2 i, \quad (1)$$

where

$$\tau_{\text{opt}} = \frac{3}{16} \sigma_{\text{T}} \int_{r_1}^{r_2} \int_{\mu_2}^{\mu_1} n(r, \mu) dr d\mu \quad (2)$$

is a mean optical depth, and

$$\gamma = \frac{\int_{r_1}^{r_2} \int_{\mu_2}^{\mu_1} n(r, \mu) \mu^2 dr d\mu}{\int_{r_1}^{r_2} \int_{\mu_2}^{\mu_1} n(r, \mu) dr d\mu} \quad (3)$$

is a ‘‘shape’’ factor. i is the clump axis inclination to the line of sight; $\mu = \cos \vartheta$, where ϑ is the clump opening angle between the axis of symmetry and the direction of the scatter seen from the center of the star; $n(r, \mu)$ is the electron number density in the clump; and σ_{T} is the Thomson scattering cross-section. For the local reference frame (r, ϑ) chosen, we let $\mu_1 = 1$. Given constant solid angle $\Delta\Omega$, the electron density is assumed to vary only with the distance, i.e., as $n(r, \mu) = n(r)$. To calculate the electron density in one clump, we use the mass conservation law:

where \dot{M}_b is the mass outflow rate within one clump, $\rho(r)$ is the mass density, and $v(r)$ is the radial velocity law that the clump will follow, which we adopt to be of the common form:

$$v(r) = v_\infty \left(1 - \frac{b R_*}{r}\right)^\beta, \quad (5)$$

where v_∞ is the terminal clump speed, R_* is the photospheric radius of the WR star (We note that there are dynamical and effective optical photosphere notations, see Brown et al. 1995), b is a dimensionless parameter to ensure that the initial wind speed is non-zero ($b = 0.995$ is adopted throughout the simulations), and β is a velocity law index, one of our basic clump parameters.

The electron density in a clump thus becomes

$$\begin{aligned} n_e &= \frac{\rho}{\mu_e m_H} \\ &= \frac{\dot{M}_b}{\mu_e m_H \Delta\Omega r^2 v} \\ &= \frac{\dot{M}_b}{\mu_e m_H \Delta\Omega r^2 v}, \end{aligned} \quad (6)$$

where m_H is the hydrogen mass, μ_e is the mean particle weight per free electron.

To deal with the finite star geometry, the point source depolarization correction factors $D(r/R_*)$, $C(r/R_*, \chi)$ can be employed according to Cassinelli et al. (1987) and Brown et al. (1989),

$$\begin{aligned} D &= \sqrt{1 - \frac{R_*^2}{r^2}} \\ &= \sqrt{1 - \frac{1}{x^2}} \end{aligned} \quad (7)$$

and

$$C = \frac{8 - D(1 + D)(1 - 3 \cos^2 \chi)}{3(1 + D)(1 + \cos^2 \chi)}, \quad (8)$$

where $x = r/R_*$, again R_* is the photospheric radius of the WR star, and χ is the scattering angle.

We wish to combine Eqs. 1 to 8 to yield an expression for the polarization from a single clump with the assumed geometry. After the dimensionless treatment of r (i.e., $r1/R_* = x1$ and $r2/R_* = x2$), the polarization expression now becomes

$$\begin{aligned} p &= \frac{3}{16} \sigma_T n_o R_* (1 - \mu_2)(\mu_2 + \mu_2^2) \sin^2 \chi \int_{x_1}^{x_2} \left(\frac{x}{x-b}\right)^\beta \frac{D(x) dx}{x^2} \\ &= \frac{3}{16} \sigma_T n_o R_* (1 - \mu_2)(\mu_2 + \mu_2^2) \sin^2 \chi \\ &\quad \times \int_{x_1}^{x_2} \left(\frac{x}{x-b}\right)^\beta \frac{1}{x^2} \sqrt{1 - \frac{1}{x^2}} dx \end{aligned} \quad (9)$$

and the scattered light intensity f_s as a fraction of $L_*/4\pi$ in terms of Brown et al. (1995) is:

$$\begin{aligned} f_s &= \frac{3}{16} \sigma_T n_o R_* (1 - \mu_2)(1 + \cos^2 \chi) \int_{x_1}^{x_2} \left(\frac{x}{x-b}\right)^\beta \frac{C(r, \chi) dx}{x^2} \\ &= \frac{3}{16} \sigma_T n_o R_* (1 - \mu_2) \\ &\quad \times \int_{x_1}^{x_2} \frac{8 - D(1 + D)(1 - 3 \cos^2 \chi)}{3(1 + D)x^2} \left(\frac{x}{x-b}\right)^\beta dx, \end{aligned} \quad (10)$$

2.2 Inference of Conservation of Electrons in A Clump

It is assumed that the clump has an initial extent of radial thickness $\Delta x = x_2 - x_1$ ($= 0.01$, for example) and solid angle $\Delta\Omega$ ($= 0.04$, for example), and the solid angle remains fixed. As the clump moves outward radially, obeying the velocity law, its thickness will naturally change to expand radially with both outer face and inner face obeying the local velocity expression. We may explicitly obtain the number of electrons in one clump

$$\begin{aligned} N_e &= \int_0^{2\pi} \int_{\mu_1}^{\mu_2} \int_{r_1}^{r_2} n_e dV \\ &= \frac{\dot{M}_b R_*}{\mu_e m_H v_\infty} \int_{x_1}^{x_2} \frac{dx}{(1-b/x)^\beta}, \end{aligned} \quad (11)$$

where $dV = -r^2 d\mu d\phi dr$ in a local spherical coordinate, and for the geometry of the clump assumed, one may get $\mu_1 = 1$ and $\Delta\Omega = 2\pi(1 - \mu_2)$.

In Eq. 11, for given values of β and initial Δx , the integral can be solved analytically and/or numerically. In the work, we adopt three acceleration cases: $\beta = 0.5$ for a rapidly accelerating flow; $\beta = 1$, a commonly assumed value for hot star winds; and $\beta = 2$ for the slow acceleration case. These are chosen so we can determine which case provides an improved fit to the WR observational properties.

(1) In case of $\beta = 0.5$, we may analytically do the integral in the Eq. 11 and obtain

$$\begin{aligned} N_e &= \frac{\dot{M}_b R_*}{\mu_e m_H v_\infty} \int_{x_1=1}^{x_2} \frac{\sqrt{x}}{\sqrt{x-b}} dx \\ &= \frac{\dot{M}_b R_*}{\mu_e m_H v_\infty} \left[\sqrt{x(x-b)} + b \ln \left(\sqrt{x} + \sqrt{x-b} \right) + \text{con1} \right]_{x_1}^{x_2} \\ &= N_{e0} \left(\sqrt{x_2(x_2-b)} - \sqrt{x_1(x_1-b)} + b \ln \frac{\sqrt{x_2} + \sqrt{x_2-b}}{\sqrt{x_1} + \sqrt{x_1-b}} \right) \\ &= N_{e0} \left[\sqrt{x(x-b)} + b \ln \left(\sqrt{x} + \sqrt{x-b} \right) + \text{con1} \right]_1^{1+0.01}, \end{aligned} \quad (12)$$

where con1 is a constant from integral and $N_{e0} = \frac{\dot{M}_b R_*}{\mu_e m_H v_\infty}$ is also a constant for given the stellar parameters. Owing to the boundary condition assumed, i.e. $x_2 = x_1 + \Delta x = 1 + 0.01$ at $x_1 = 1$, the expression $\left[\sqrt{x(x-b)} + b \ln \left(\sqrt{x} + \sqrt{x-b} \right) + \text{con1} \right]_1^{1+0.01}$ equals to 0.103. Therefore, Eq. 12 can clearly yield the following equation

$$\sqrt{x_2(x_2-b)} - \sqrt{x_1(x_1-b)} + b \ln \frac{\sqrt{x_2} + \sqrt{x_2-b}}{\sqrt{x_1} + \sqrt{x_1-b}} = 0.103. \quad (13)$$

(2) In case of $\beta = 1$, we use the same method above and get the equation

$$x_2 - x_1 + b \ln \frac{x_2 - b}{x_1 - b} = 1.103. \quad (14)$$

(3) In case of $\beta = 2$, we repeat the same process and obtain the following equation

$$x_2 - x_1 + 2b \ln \frac{x_2 - b}{x_1 - b} + \frac{b^2(x_2 - x_1)}{(x_1 - b)(x_2 - b)} = 134.2. \quad (15)$$

Eq. 13, 14, or 15 sets up the coherent relationship between x_1 and x_2 . We may use them with a given value of β to get x_2 once x_1 is specified. In the simulations, we use the Newtonian bisection and bracketing methods to solve the Eq. 13, 14, or 15 due to the nonlinear relationship between x_1 and x_2 . Note, it is clearly shown that the number of electrons in a clump with various β are different ($N_e = N_{e0} \times 0.103$ for $\beta = 0.5$, $N_e = N_{e0} \times 1.103$ for $\beta = 1$ and $N_e = N_{e0} \times 134.2$ for $\beta = 2$). [We may also have a special case of $\beta = 0$, which will give the value of the integral equals to Δx ($\Delta x=0.01$) and then we will have the expression $N_e = N_{e0} \times 0.01$ for $\beta = 0$.] The electron scattering in the clump results in the polarization,

2.3 Relation between Time t since Clump Expulsion and the Clump Distance r from the Star

The radial thickness varies with time as the clump moves out. We can connect the time since expulsion of a particular clump with its current radial distance together from the velocity law. Similarly, given time t , the clump distance (say r) can be obtained. From the clump velocity law, this relationship is,

$$\begin{aligned} t &= \int \frac{dr}{v(r)} \\ &= \frac{R_*}{v_\infty} \int \frac{dx}{(1-b/x)^\beta} \\ &= \tau \int \frac{dx}{(1-b/x)^\beta}, \end{aligned} \quad (16)$$

where $\tau = R_*/v_\infty$ is denoted as the ‘‘flow time scale’’.

Again, in the case of $\beta = 0.5$,

$$\begin{aligned} \frac{t}{\tau} &= \int \frac{\sqrt{x}}{\sqrt{x-b}} dx \\ &= \sqrt{x(x-b)} - \frac{b}{2} \ln \left[\frac{x-b}{b} \left(\sqrt{\frac{x}{x-b}} - 1 \right)^2 \right] + \text{con2}. \end{aligned} \quad (17)$$

If we adopt $x = 1$ at $t = 0$ and use $b = 0.995$ so far, then we will get $\text{con2} = -0.14$ in the Eq. 17. Therefore, the expression between time and distance is

$$\frac{t}{\tau} = \sqrt{x(x-b)} - \frac{b}{2} \ln \left[\frac{x-b}{b} \left(\sqrt{\frac{x}{x-b}} - 1 \right)^2 \right] - 0.14. \quad (18)$$

In the cases of $\beta = 1$ and $\beta = 2$, the expression between time and distance are, respectively,

$$\frac{t}{\tau} = x + b \ln(x-b) + 4.27 \quad (19)$$

and

$$\frac{t}{\tau} = x - b + 2b \ln(x-b) - \frac{b^2}{x-b} + 208.55. \quad (20)$$

Therefore, from the numerical experiments, t/τ may be stepwise accumulated by doing summation of $\Delta t/\tau$, and $\Delta t/\tau$ is chosen to have a Gaussian distribution.

2.4 Polarization for An Ensemble of Clumps

The expressions above for polarization and scattering are for a single clump. For accounting for many clumps, we use the same approach as in Li et al. (2000). We set up a spherical coordinate system (r, θ, ϕ) with the polar axis oz being along the line of sight. Then for each clump the ‘‘inclination’’ angle i is identical to both the scattering angle χ and the polar angle θ , while the polarization position angle in the sky, ψ , is just the coordinate component ϕ (see Fig. 1).

For a system of clumps labeled $j = 1, N$, the total scattered light fraction f_s and the net polarization are as usual for the optically thin case, simply given by the sum over j the Stokes intensity parameters $Q_j = p_j \cos 2\phi_j$, $U_j = p_j \sin 2\phi_j$ of each to get the totals of Q and U , then finding $p = (Q^2 + U^2)^{1/2}$ and position angle $\Psi = \frac{1}{2} \arctan \frac{U}{Q}$. It is to be understood that *summations exclude all occulted clumps* – i.e. clumps whose coordinates x_j, θ_j, ϕ_j satisfy $\theta_j > \pi/2$ and $x_j \sin \theta_j < 1$. Note that $\mu_j = \cos \theta_j$ is uniformly sampled in the interval -1 to $+1$ and ϕ_j from 0 to 2π . The radii x_j are determined by time and the velocity law.

The total mass loss rate \dot{M} is distributed among all clumps and the ambient, inhomogeneous but, on average, spherical ‘‘wind’’. We choose the fraction of the mass loss in the clumps to be η . Hence, $\eta \dot{M} = \dot{N} N_e \mu_e m_H$, where \dot{N} is the mean clump ejection rate (s^{-1}) and N_e again is the total number of electrons in one clump. Thus, if we fix \dot{M} and increase \dot{N} then there are more clumps in any given range of r but each would be of smaller N_e . We denote $\mathcal{N} = \dot{N} \tau$, the number of clumps ejected per characteristic flow time ($\tau = R_*/v_\infty$), as the measure of the clump ejection rate. If we assume the portion of the total mass loss rate

$\eta\dot{M} = k\dot{M}_b$. Since in a flow time τ , there are \mathcal{N} clumps ejected, we can attain $k \sim \mathcal{N}$. Therefore, we may replace \dot{M}_b in Eq. 6 with $\eta\dot{M}/\mathcal{N}$ when accounting for many clumps in the simulations.

The system of equations governing the time varying polarization and scattered light is then

$$\begin{aligned}
Q &= \sum_{j=1}^N Q_j \\
&= \frac{3}{16} \sigma_{\text{T}} n_o R_* (1 - \mu_2)(\mu_2 + \mu_2^2) \sum_{j=1}^N \sin^2 \theta_j \cos 2\phi_j \\
&\quad \times \int_{x_1}^{x_2} \left(\frac{x_j}{x_j - b} \right)^\beta \frac{1}{x_j^2} \sqrt{1 - \frac{1}{x_j^2}} dx_j \\
&= \frac{3}{16} \sigma_{\text{T}} \frac{n'_o}{\mathcal{N}} R_* (1 - \mu_2)(\mu_2 + \mu_2^2) \sum_{j=1}^N \sin^2 \theta_j \cos 2\phi_j \\
&\quad \times \int_{x_1}^{x_2} \left(\frac{x_j}{x_j - b} \right)^\beta \frac{1}{x_j^2} \sqrt{1 - \frac{1}{x_j^2}} dx_j \\
&= \frac{p_0}{\mathcal{N}} \sum_{j=1}^N \sin^2 \theta_j \cos 2\phi_j \int_{x_1}^{x_2} \left(\frac{x_j}{x_j - b} \right)^\beta \frac{1}{x_j^2} \sqrt{1 - \frac{1}{x_j^2}} dx_j
\end{aligned} \tag{21}$$

and

$$\begin{aligned}
U &= \sum_{j=1}^N U_j \\
&= \frac{3}{16} \sigma_{\text{T}} n_o R_* (1 - \mu_2)(\mu_2 + \mu_2^2) \sum_{j=1}^N \sin^2 \theta_j \sin 2\phi_j \\
&\quad \times \int_{x_1}^{x_2} \left(\frac{x_j}{x_j - b} \right)^\beta \frac{1}{x_j^2} \sqrt{1 - \frac{1}{x_j^2}} dx_j \\
&= \frac{3}{16} \sigma_{\text{T}} \frac{n'_o}{\mathcal{N}} R_* (1 - \mu_2)(\mu_2 + \mu_2^2) \sum_{j=1}^N \sin^2 \theta_j \sin 2\phi_j \\
&\quad \times \int_{x_1}^{x_2} \left(\frac{x_j}{x_j - b} \right)^\beta \frac{1}{x_j^2} \sqrt{1 - \frac{1}{x_j^2}} dx_j \\
&= \frac{p_0}{\mathcal{N}} \sum_{j=1}^N \sin^2 \theta_j \sin 2\phi_j \int_{x_1}^{x_2} \left(\frac{x_j}{x_j - b} \right)^\beta \frac{1}{x_j^2} \sqrt{1 - \frac{1}{x_j^2}} dx_j,
\end{aligned} \tag{22}$$

where $n'_o = \eta\dot{M}/(\mu_e m_H \Delta\Omega R_*^2 v_\infty)$ and

$$\begin{aligned}
p_0 &= \frac{3}{16} \sigma_{\text{T}} n'_o R_* (1 - \mu_2)(\mu_2 + \mu_2^2) \\
&= \frac{3}{16} \sigma_{\text{T}} \frac{\eta\dot{M}}{\mu_e m_H \Delta\Omega R_*^2 v_\infty} R_* (1 - \mu_2)(\mu_2 + \mu_2^2).
\end{aligned} \tag{23}$$

Hence, the total polarization is given

$$p = \sqrt{Q^2 + U^2} \tag{24}$$

and

$$f_{\text{s}} = \sum_{i=1}^N f_{\text{si}}$$

$$\begin{aligned}
&= \frac{3}{16} \sigma_T n_o R_* (1 - \mu_2) \\
&\quad \times \sum_{j=1}^N \int_{x_1}^{x_2} \frac{8 - D_j(1 + D_j)(1 - 3 \cos^2 \theta_j)}{3(1 + D_j)x_j^2} \left(\frac{x_j}{x_j - b} \right)^\beta dx_j \\
&= \frac{3}{16} \sigma_T \frac{n'_o}{\mathcal{N}} R_* (1 - \mu_2) \\
&\quad \times \sum_{j=1}^N \int_{x_1}^{x_2} \frac{8 - D_j(1 + D_j)(1 - 3 \cos^2 \theta_j)}{3(1 + D_j)x_j^2} \left(\frac{x_j}{x_j - b} \right)^\beta dx_j \\
&= \frac{f_0}{\mathcal{N}} \sum_{j=1}^N \int_{x_1}^{x_2} \frac{8 - D_j(1 + D_j)(1 - 3 \cos^2 \theta_j)}{3(1 + D_j)x_j^2} \left(\frac{x_j}{x_j - b} \right)^\beta dx_j, \tag{25}
\end{aligned}$$

where

$$\begin{aligned}
f_0 &= \frac{3}{16} \sigma_T n'_o R_* (1 - \mu_2) \\
&= \frac{3}{16} \sigma_T \frac{\eta \dot{M}}{\mu_e m_H \Delta \Omega R_*^2 v_\infty} R_* (1 - \mu_2). \tag{26}
\end{aligned}$$

Note again, in the above expressions, both x_1 and x_2 are varying with time, so we need to use Eq. 13, 14, or 15 in regards to various β to determine x_2 once x_1 is given. Here, x_1 is obtained from Eq. 18, 19, or 20 in case of different β , if time t is known from the numerical experiments.

On inspection of the above equations for polarization and scattered light, we expect that, for given \dot{M} , $\Delta \Omega$, initial Δr , and β , results should depend mainly on \mathcal{N} . For a fixed mass loss rate and flow time, if the clump generation rate is low, only a few clumps each of large density will be present near the star and these dominate the p and f_s values, as is shown in Li et al. (2000). But for high generation rates, many low density clumps near the star will be controlling p and f_s . So the same total number of electrons is redistributed in different number of clumps, resulting in different statistical means and variances in the polarization and scattered light fraction. For a fixed clump ejection and mass loss rate, the number of clumps in the inner radii near the star has a steady mean value and so therefore do the resulting polarization, scattered intensity and their variances, but these values change with \mathcal{N} , \dot{M} , and β . So their observed values allow inference of the clump emission and flow parameters.

3 MODEL RESULTS AND DISCUSSION

1. As a start, let us calculate the thickness, volume and polarization of a single clump with varying clump location, supposing $\sin \chi = 1$ and $\beta = 1$. The results are displayed in Fig 2. In Fig.2a the solid line denotes the inner radial boundary (say x_1) and the dotted line denotes the outer radial boundary (say x_2). We see that as the time progresses, x_2 increases faster than x_1 , which directly induces the thickness expansion. In Fig.2a, as for comparison, x_2 ($x_2 = x_1 + \Delta x$) with the constant thickness $\Delta x = 0.01$ is shown in the dashed line which almost overlaps the solid line x_1 . In Fig.2b, the solid line denotes the case for which a constant clump thickness is assumed. In contrast, the dotted line shows the expansion of the thickness with its location (i.e. x), and we see that the thickness increases rapidly among $x = 1$ to $x = 2$, where the winds are mainly accelerated. In Fig.2c, the solid line denotes the volume of the clump with constant thickness $\Delta x = 0.01$ and the dotted line denotes the volume of the clump with expanding thickness, which is increasing dramatically faster than the constant thickness case. We compare the polarization of varying thickness (the dotted line in Fig.2d) with that in the Davies et al. (the solid line in Fig.2d) for one single clump and see that in both cases, the polarization decreases as the clump moves outward, while there is a peak polarization about $x = 1.2$ for the latter case.
2. Furthermore, we calculate the thickness, volume and polarization of a single clump with varying clump location, supposing $\sin \chi = 1$ but with different β , as is shown in Fig.3. To see how the x_1 varies with time (say t/τ) in case of differing β s, we show the results in Fig.3a in which fast acceleration of $\beta = 0.5$ is displayed in dashed line and moderate acceleration of $\beta = 1$ is in solid line, and slow acceleration of $\beta = 2$ is in dash-dotted line. We also show the radial thickness varies with location of the clump in Fig.3b. The dash-dotted line denotes the case of $\beta = 2$, the solid line denotes the case of $\beta = 1$, and the dashed line denotes the case of $\beta = 0.5$. In addition, we show the constant thickness case with $\beta = 1$ in dotted line. In Fig.3c, we show that the volume changes with the clump location in various cases of β as denoted in the figure. In Fig.3d, we show the polarization varies with location of the clump. The dash-dotted line denotes the case of $\beta = 2$, the solid line denotes the case of $\beta = 1$, and the dashed line

the start values of polarization in various case of β are different since the electron number in one single clump for various case of β is different, as is shown from Eq. 12 which is related to β . And polarization is mainly determined by the number of electrons in the clump (Brown et al. 1995).

3. Taking into account the behavior of an ensemble of clumps, we compute the polarization, the fraction of scattering light intensity, and their variation. In particular, we calculate the ratio of their variations for various clump ejection rate \mathcal{N} in a flow time with various $\beta = 0.5, 1, 2$. Interestingly, σ_p/\bar{p} and $\sigma_p/\sigma_{\text{phot}}$ do not depend on any specific star, but only on the \mathcal{N} and β . It is not surprising at this since p (or f_s) linearly relies on p_0 (or f_0) which is determined by the stellar parameters of a star. So we enable to treat $\sigma_p/\sigma_{\text{phot}}$ as a probe to explore the probable \mathcal{N} and β . To get rid of the influence of any specific star, we divide p (as well as Q and U) in Eq. 24 by p_0 in Eq. 23 and divide f_s in Eq. 25 by f_0 in Eq. 26. The results are displayed in Tables 1, 2 and 3. Using the values in these tables, we plot σ_p/\bar{p} and $\sigma_p/\sigma_{\text{phot}}$ with various \mathcal{N} in cases of various $\beta = 0.5, 1, 2$. The observed value of $\sigma_p/\bar{p} = 0.5$ is denoted in dotted line in the upper panel of Fig. 4, and the observed value of $\sigma_p/\sigma_{\text{phot}} = 0.05$ is denoted in dotted line in the lower panel of Fig. 4. We found that to achieve the observed value, three patterns could hold, for $\beta = 0.5 \rightarrow \mathcal{N} \sim 500$; for $\beta = 1 \rightarrow \mathcal{N} \sim 150$; and for $\beta = 2 \rightarrow \mathcal{N} \sim 1$. Although there seems no solid unique solution for β and \mathcal{N} in terms of the above considerations, while combining the effects of \mathcal{N} and β on $\sigma_p/\sigma_{\text{phot}}$ and f_V the volume filling factor, it seems the observed data might prefer the case of $\mathcal{N} = 1$ and $\beta = 2$. We will further demonstrate this later.

Hamann and Koesterke (1998) found the clump volume filling factor of WR subtype WN stars about 30% in terms of their spectrum analyses. In the work of the paper, we are able to calculate the clump volume filling factor from our model. After doing summations of volumes that all clumps occupy and divided it by the whole space accounted for, then the volume filling factor denoted as f_V , can in common definition be obtained,

$$f_V = \frac{\sum_{i=1}^{\mathcal{N}} \Delta V_i}{\frac{4\pi}{3}(r^3 - R_*^3)}. \quad (27)$$

We present the model results of f_V in column 9 of Tables 1, 2 and 3 in case of various β s. We also plot f_V vs \mathcal{N} in Fig. 5, in which the dotted line denotes the ‘‘observed’’ of 30%. The figure shows $\beta = 0.5 \rightarrow \mathcal{N} \sim 700$; $\beta = 1 \rightarrow \mathcal{N} \sim 100$; $\beta = 2 \rightarrow \mathcal{N} \sim 1$, in regards to the observed. Note, f_V greater than 1 means clumps overlapped or merged. So for the assumption of thin clumps, we would rule out the cases of $f_V > 1$.

In general, the hot star winds show two-component property: the smooth ambient and clumps. Of course, when the clumps move outward to very far away distance, they will become as part of the interstellar medium. However, the density of clumps is in fact higher than that of the ambient wind around the star within several hundred of stellar radius. The smaller the value of the volume filling factor, the stronger the wind clumping. A clumping wind may cause higher emission for the same amount of material, which implies that the mass loss rates by spectroscopic analysis under the assumption of a smooth wind are systematically overestimated by typically a factor of $\frac{1}{\sqrt{f_V}} \sim 2$ and even higher, and the mass loss rates in turn consequently affect the stellar structure and evolution. Such clumping presumably arises from the inherent instability of radiation driven winds and would influence the strength of the electron scattering wings, change ionization and line ratios, and cause polarization variability and profile variability. In fact, Abbott et al. (1981) has taken the inhomogeneities (i.e. clumps) in the wind into account and got the relationship of the mass loss rate, radio flux, and the filling factor. Later, in most of models, in most simplicity, the inter-clump medium is usually treated as void, which recently leads to the porous scenario (Owocki and Cohen, 2006) for OB stars, as the photons are able to leak freely through the large separation between clumps. However, our model clearly indicates that the void treatment for WR stars might likely cast some doubts, since the inter-clump medium, occupying a very large mass percentage of the total, may play a role in the hot wind emission, in particular, near the star. The whole inter-clump medium, being of the smooth spherical wind ambient, globally contributes nil to the net polarization due to the cancellation effect of polarization.

4. We compute the photometric and polarimetric intensity and their fluctuations in case of various β s. Figs. 6, 8 and 10 show how polarization, position angle, and scattered light intensity change with the total number of clumps emitted from the start. Polarization changes are also shown as a locus in the Q–U plane (see Figs. 6, 8 and 10) which, as expected, shows no strong preferred direction, since the mean structure is quasi-spherical. In Figs. 7, 9, and 11 we show ‘‘observational’’ time-smoothed results for the variations in mean polarization and scattered light. Standard deviations, σ , of these quantities are also plotted in these figures. The ratio \mathcal{R} versus total number of clumps \mathcal{N} as time progresses is plotted in Fig. 12, from which we see that in order to obtain the *sustainable* $\mathcal{R} = 0.05$ as observed, the pattern of $\beta = 2$ and $\mathcal{N} = 1$ is indeed preferred. This seems comparable to the number of subpeaks of the broad line observed. Given the model quantities $R_* = 10R_\odot$ and $v_\infty = 1800 \text{ km s}^{-1}$, the flow time τ is about

new clumps will occur. Hence, there would consequently result in 10 more detectable subpeaks since the clump emission is dominated by the inner clumps in the line emission regions (LER), which are closer to the star. This conclusion is indeed consistent with the observations and their analysis (Robert 1992, Brown et al. 1995). Note, envisaging Tables 1, 2 and 3 in which $\mathcal{R} = 0.05$ seem to be attained, however, observing Figs. 6, 8, 10, and their time averaged results in Figs. 7, 9, 11, in particular 12, we found that *only* the case of $\beta = 2$ and $\mathcal{N} = 1$ shows a real and sustainable result. Neither the case of $\beta = 1$ and $\mathcal{N} = 200$, nor the case $\beta = 0.5$ and $\mathcal{N} = 1000$, could achieve a long-standing $\mathcal{R} = 0.05$. Therefore, we have to abandon these cases. If we plot the number of clumps versus the distance (Fig. 13), we will find that in case of various $\beta = 0.5, 1, 2$ but with same $\mathcal{N} = 1$, there will several hundred of clumps radially staggering outward from $1R_*$ to $5R_*$ in case of $\beta = 2$ being very slowly accelerated, but just a few in case of $\beta = 0.5, 1$ being rapidly accelerated. In terms of the concept of LER in Lepine & Moffat (1999) and Dessart & Owocki (2005), the LER with velocity space is about among $0.4\text{--}0.9v_\infty$ where the clumps are accelerated. We note that the WR-wind acceleration length scale $\beta R_* \sim 20R_\odot$ in their results, is compatible with our results, with $R_* = 10R_\odot$ applied and $\beta = 2$ inferred.

5. For the fraction factor of the mass loss rate into the clumps η in regards to p_0 in Eq. 23 and f_0 in Eq. 26, we could use the typical polarization observed for WR stars $\bar{p} = 0.1 - 1\%$ to constrain it. If the following typical parameters are employed: $\dot{M} = 2.5 \times 10^{-6} M_\odot/\text{year}$, $\Delta\Omega = 0.04$, initial $\Delta r_0 = 0.01R_*$, $\mu_e = 2$, $R_* = 10R_\odot$ and $v_\infty = 1800 \text{ km s}^{-1}$, then we may gain $p_o = 0.0147\eta$. From the above discussion, the pattern $\beta = 2$ and $\mathcal{N} = 1$ is preferred, then we check Table 3 and get $\bar{p}' = \bar{p}/p_o \sim 124.85 \rightarrow \bar{p} = 1.84\eta$. Therefore, we enable to gain $\eta = \bar{p}/1.84 \sim 10^{-3} - 10^{-2}$. This would imply that only a quite small portion of the winds is going to deposit into the clumps but most of winds are blown as an ambient where clumps embedded. In contrary, one might recall the solar wind picture in which the solar wind is a coherent outward expansion of the solar corona, frequently involving the corona mass ejection (CME) events. Hence, it is not surprising that there are two components in the hot star environments, being the ambient winds and the clumps (or wind-blown bubbles). However, the formation mechanisms of the solar winds and hot star winds are distinctly different. The former is driven by the gas pressure gradient of the high temperature solar corona, and the latter is driven by the pressure of the radiation emitted by the hot star, so-called the continuum-driven and line-driven. Note that the physical quantities in Tables 1, 2 and 3, such as $\bar{p}' = \bar{p}/p_o$, $\sigma'_p = \sigma_p/p_o$, $\bar{f}'_s = \bar{f}_s/f_o$, $\sigma'_{\text{phot}} = \sigma_{\text{phot}}/f_o$, \bar{p}/\bar{f}_s , $\sigma_p/\sigma_{\text{phot}}$, scale with p_o or f_o , so they are dimensionless numbers. The fraction factor η only affects the values of p_o and f_o . Thus for a specific star one could gain η incorporating the stellar parameters and observed polarization. We realize that the clumps ejected in our model are massive- or macro-clumps, distinguished from the local perturbations in the winds.

4 CONCLUSIONS

In this paper, we update the previous model proposed by Li et al. (2000) and apply the clump ejection scenario to explain the WR star wind polarization and its variability observed, by accounting for the expansion of the clumps along the wind flows but keeping the solid angle constant. We may gain the main conclusions as follows.

(1) From numerous model simulations using various β and \mathcal{N} , incorporating with the volume filling factor f_V , we found $\beta \sim 2$ and $\mathcal{N} \sim 1$ are preferred for explaining the observational data on photometric, polarimetric, and spectral line profile variability of WR stars. This gives well model constraints on the stellar wind properties of hot stars.

(2) We also found that a small fraction as 10^{-3} of the wind material deposits into the clumps but most of the mass loss are going to the space as wind ambient. This quantitative estimation of the mass fraction into the wind ambient implies that the porous wind models for WR stars might be cautious since the inter-clump medium is far from void.

In summary, this updated model which is improved from Li et al. 2000, with inclusion of the radial expansion of the thickness of clumps but retaining the dependence on the β velocity law and stellar occultation effects, yields results consistent with observations in regards to the mean polarization \bar{p} , the ratio $\mathcal{R} = \sigma_p/\sigma_{\text{phot}}$ of polarimetric to photometric variability, and the volume filling factor f_V . It offers a quantitative estimation of the mass fraction into the clumps and ambient winds as well. Hence, the model produces a valuable diagnostic of WR wind structure.

Acknowledgements We would like to thank the anonymous referee for the constructive comments that led to a significant improvement in the paper. The authors would like to thank Ben Davies for informative discussion for the work. The authors acknowledge support for this work from: the Natural Science Foundation of China grants 10273002, 10573022, and 10778601 (QL); the NSF Center for Magnetic Self Organization in Laboratory and Astrophysics Plasmas (JPC); UK STFC Rolling Grant (JCB). JPC and RI have been partially supported by the STFC grants ST/S000100/1 and ST/S000100/2.

Table 1 Simulation results for finite star source with occultation and velocity law with $\beta = 0.5$

N	\mathcal{N}	\bar{p}'	σ'_p	\bar{f}'_s	σ'_{phot}	\bar{p}'/\bar{f}'_s	$\sigma_p/\sigma_{\text{phot}}$	f_V
5000	1/4	0.8394	0.8632	4.928	4.470	0.337	0.382	0.0001
5000	1	0.3565	0.2032	2.319	1.138	0.305	0.353	0.0003
5000	5	0.1557	0.0816	1.927	0.276	0.160	0.479	0.0016
5000	10	0.1091	0.0557	1.891	0.234	0.114	0.473	0.0033
5000	50	0.0500	0.0265	1.835	0.195	0.054	0.271	0.0164
5000	100	0.0364	0.0204	1.783	0.239	0.040	0.168	0.0328
5000	200	0.0268	0.0146	1.693	0.304	0.031	0.094	0.0654
5000	1000	0.0143	0.0051	1.229	0.424	0.023	0.024	0.3190
5000	2000	0.0102	0.0031	0.910	0.392	0.022	0.016	0.6239

Notes: Column 1 is the total number of clumps applied in the simulations. Column 2 is the clump ejection rate in a flow time. Column 3 is $\bar{p}' = \bar{p}/p_0$. Column 4 is $\sigma'_p = \sigma_p/p_0$. Column 5 is $\bar{f}'_s = \bar{f}_s/f_0$. Column 6 is $\sigma'_{\text{phot}} = \sigma_{\text{phot}}/f_0$. Column 7 is \bar{p}'/\bar{f}'_s . Column 8 is $\sigma_p/\sigma_{\text{phot}}$. Column 9 is the volume filling factor f_V .

References

- Abbott, D. C., Biegging, J. H., & Churchwell, E. 1981, *ApJ*, 250, 645
- Brown, J. C. 1994, in: Quebec Workshop on Instability and Variability in Hot Star Winds. Eds. Moffat, A.F.J. and St-Louis, N., APSS, 221,357
- Brown, J. C. & McLean, I. S. 1977, *A&A*, 57, 141
- Brown, J. C., Carlaw, V. A., & Cassinelli, J. P. 1989, *AJ*344, 341
- Brown, J. C., Ignace, R., Cassinelli, J. P. 2000, *A&A*, 356, 619
- Brown, J. C., Richardson, L. L., Antokhin, I., Robert, C., Moffat, A. F. J., St-Louis, N. 1995, *A&A*295,725
- Brown, J. C., Richardson, L. L., Ignace, R., Cassinelli, J. P. 1998, *A&A*, 330, 253
- Brown, J. C., Cassinelli, J. P., Li, Q., Kholtygin, A. F., & Ignace, R. 2004, *A&A*, 426, 323
- Cassinelli, J. P., Nordsieck, K. H., Murison, M. A. 1987, *ApJ*, 317, 290
- Cassinelli, J. P., Ignace, R., Waldron, W.L., Cho, J., Murphy, N. A., & Lazarian, A. 2008, *ApJ*, 683, 1052
- Davies, B., Vink, J.S., & Oudmaijer, R.D. 2007, *A&A*, 469, 1045
- Dessart, L. & Owocki, S.P. 2005, *A&A*, 432, 281
- Drissen, L., St.-Louie, N., Moffat, A. F. J., Bastien, P. 1987, *ApJ*, 322, 888
- Drissen, L., Robert, C., Moffat, A. F. J. 1992, *ApJ*, 386, 288
- Hamann, W.R., & Koesterke, L. 1998, *A&A*, 335, 1003
- Ignace, R., Quigley, M. F., & Cassinelli, J. P. 2003, *ApJ*, 596, 538
- Lepine, S., Moffat, A. F. J., 1999, *ApJ*, 514, 909
- Lepine, S., Moffat, A.F.J., St-Louis, N., Marchenko, S.V., Dalton, M.J., Crowther, P.A., Smith, L.J., Willis, A.J., Antokhin, I.I., & Tovmassian, G.H. 2000, *AJ*, 120, 3201
- Li, Q., Brown, J. C., Ignace, R., Cassinelli, J. P., & Oskinova, L. M. 2000, *A&A*, 357, 233
- Lupie, O. L., Nordsieck, K. H. 1987, *AJ*, 92, 214
- Marchenko, S. V., Moffat, A. F. J., St-Louis, N., & Fullerton, A. W. 2006, *ApJ*, 639, L75
- Moffat, A. F. J, Robert, C. 1992, *ASP #22*, 203
- Oskinova, L.M., Hamann, W.-R., & Feldmeier, A. 2007, *A&A*, 476, 1331
- Owocki, S. P., Cohen, D. H. 2006, *ApJ*, 648, 565
- Richardson, L. L., Brown, J. C., Simmons, J. F. L. 1996, *A&A*, 306, 519
- Robert, C. 1992, Ph.D. Thesis, Univ. de Montreal
- Robert, C., Moffat, A. F. J., Bastien, P., Drissen, L., St.-Louie, N. 1989, *ApJ*, 347, 1034
- St.-Louis, N., Drissen, L., Moffat, A. F. J., Bastien, P., Tapia, S. 1987, *ApJ*, 322, 870
- Taylor, M., Nordsieck, K. H., Schulte-Ladbeck, R. E., Bjorkman, K. S. 1991, *AJ*, 102, 1187

Table 2 Simulation results for finite star source with occultation and velocity law with $\beta = 1$

N	\mathcal{N}	\bar{p}'	σ'_p	f'_s	σ'_{phot}	\bar{p}'/f'_s	$\sigma_p/\sigma_{\text{phot}}$	f_V
5000	1/4	2.8922	2.1003	22.762	17.995	0.252	0.231	0.0015
5000	1	1.4512	0.7755	15.340	5.933	0.187	0.259	0.0035
5000	5	0.6270	0.3205	14.144	2.371	0.088	0.268	0.0175
5000	10	0.4432	0.2223	14.077	1.753	0.062	0.251	0.0350
5000	50	0.2066	0.1172	13.805	1.664	0.030	0.140	0.1725
5000	80	0.1641	0.0982	13.565	1.985	0.024	0.098	0.2727
5000	100	0.1458	0.0904	13.395	2.170	0.022	0.082	0.3381
5000	150	0.1189	0.0703	13.021	2.557	0.018	0.054	0.4962
5000	200	0.1054	0.0510	12.663	2.852	0.016	0.035	0.6460
5000	400	0.0788	0.0279	11.316	3.529	0.014	0.016	1.1568
5000	1000	0.0506	0.0153	8.065	3.647	0.013	0.008	2.2168
5000	2000	0.0255	0.0088	4.986	2.591	0.010	0.007	4.0601

Notes: Parameters have the same meaning as that in Table 1.

Table 3 Simulation results for finite star source with occultation and velocity law with $\beta = 2$

N	\mathcal{N}	\bar{p}'	σ'_p	f'_s	σ'_{phot}	\bar{p}'/f'_s	$\sigma_p/\sigma_{\text{phot}}$	f_V
5000	1/4	247.339	126.392	17517.453	3157.450	0.028	0.079	0.1071
5000	1	124.8503	64.1338	17300.174	1918.061	0.014	0.066	0.4098
5000	5	48.1358	28.5260	16625.262	2933.660	0.006	0.019	1.7094
5000	10	33.3430	17.1025	15757.138	3900.831	0.004	0.009	2.6139
5000	50	14.3191	3.7360	9381.283	4799.212	0.003	0.002	1.3993
5000	80	9.6549	2.6050	6372.940	3492.983	0.003	0.002	3.3746
5000	100	7.8479	2.1951	5201.766	2891.146	0.003	0.002	5.6845
5000	150	5.2524	1.4971	3550.873	2009.073	0.003	0.002	12.349
5000	200	3.8611	1.0675	2689.970	1536.053	0.003	0.001	11.362
5000	400	1.9001	0.5064	1352.113	778.007	0.003	0.001	15.412
5000	1000	0.7599	0.2026	540.961	311.203	0.008	0.001	15.406
5000	2000	0.3800	0.1013	270.565	155.602	0.003	0.001	15.396

Notes: Parameters have the same meaning as that in Table 1.

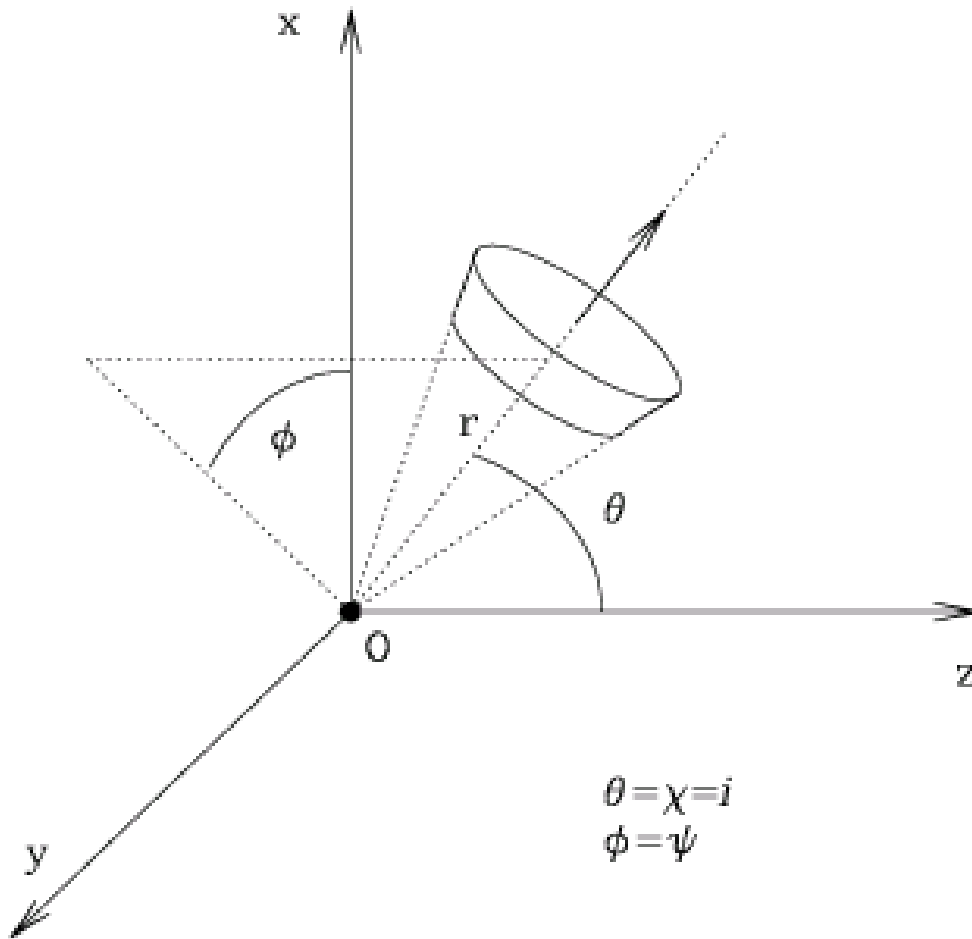


Fig. 1 Geometry of scattering from one clump. We employ a spherical coordinate system (r, θ, ϕ) with oz along the line of sight. For each clump the “inclination” angle i is identical to the scattering angle χ as well as the polar angle θ , while the polarization position angle on the sky, ψ , is the coordinate component ϕ (see Li et al. 2000).

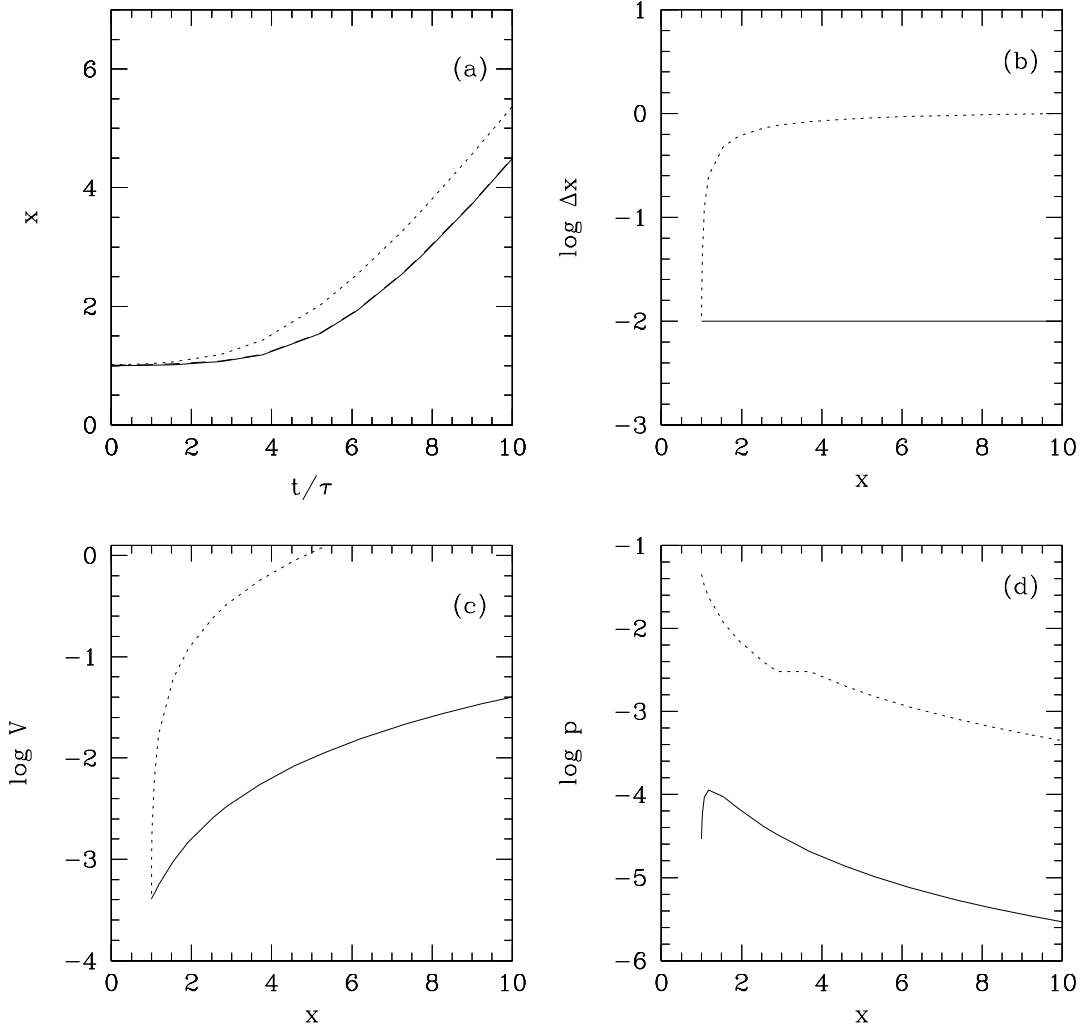


Fig. 2 Model results are shown for a single clump: (a) The radial extent vs time. The solid line denotes the inner radial boundary (say x_1) and the dotted line denotes the outer radial boundary, x_2 ($x_2 = x_1 + \Delta x$) with the constant thickness $\Delta x = 0.01$, is shown in the dashed line which is almost overlap the solid line x_1 . (b) The clump thickness versus the clump location. The solid line denotes the constant clump thickness as assumed. In contrast, the dotted line shows the expansion of the thickness with its location (i.e. x). (c) The clump volume vs its location. The solid line denotes the volume of the clump with constant thickness $\Delta x = 0.01$ and the dotted line denotes the volume of the clump with expanding thickness. (d) Polarization vs the clump location. The dotted line is for the varying thickness and the solid line is for the constant thickness as in Davies et al (2007).

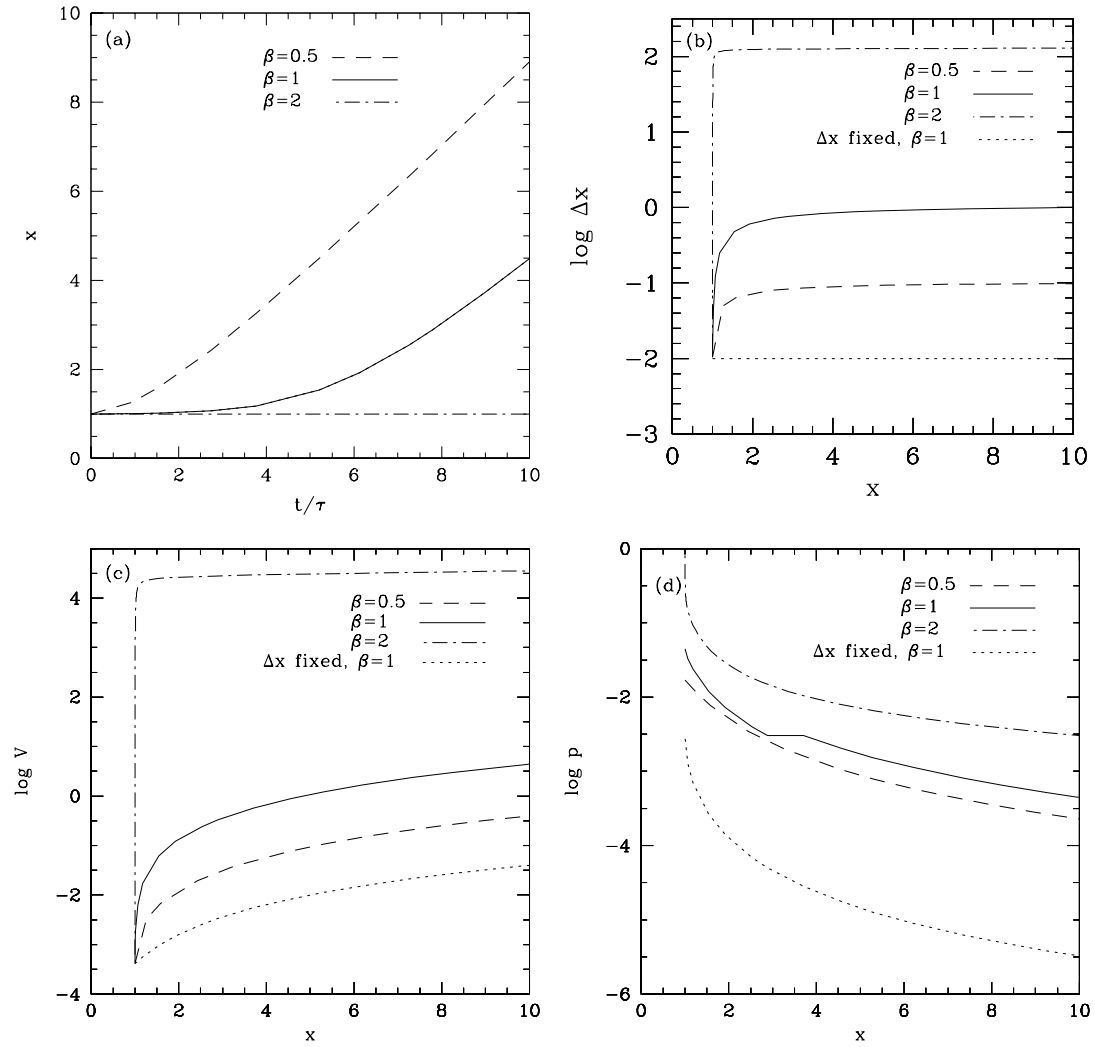


Fig. 3 Model results are displayed in various cases of β as denoted in the figure for one single clump.

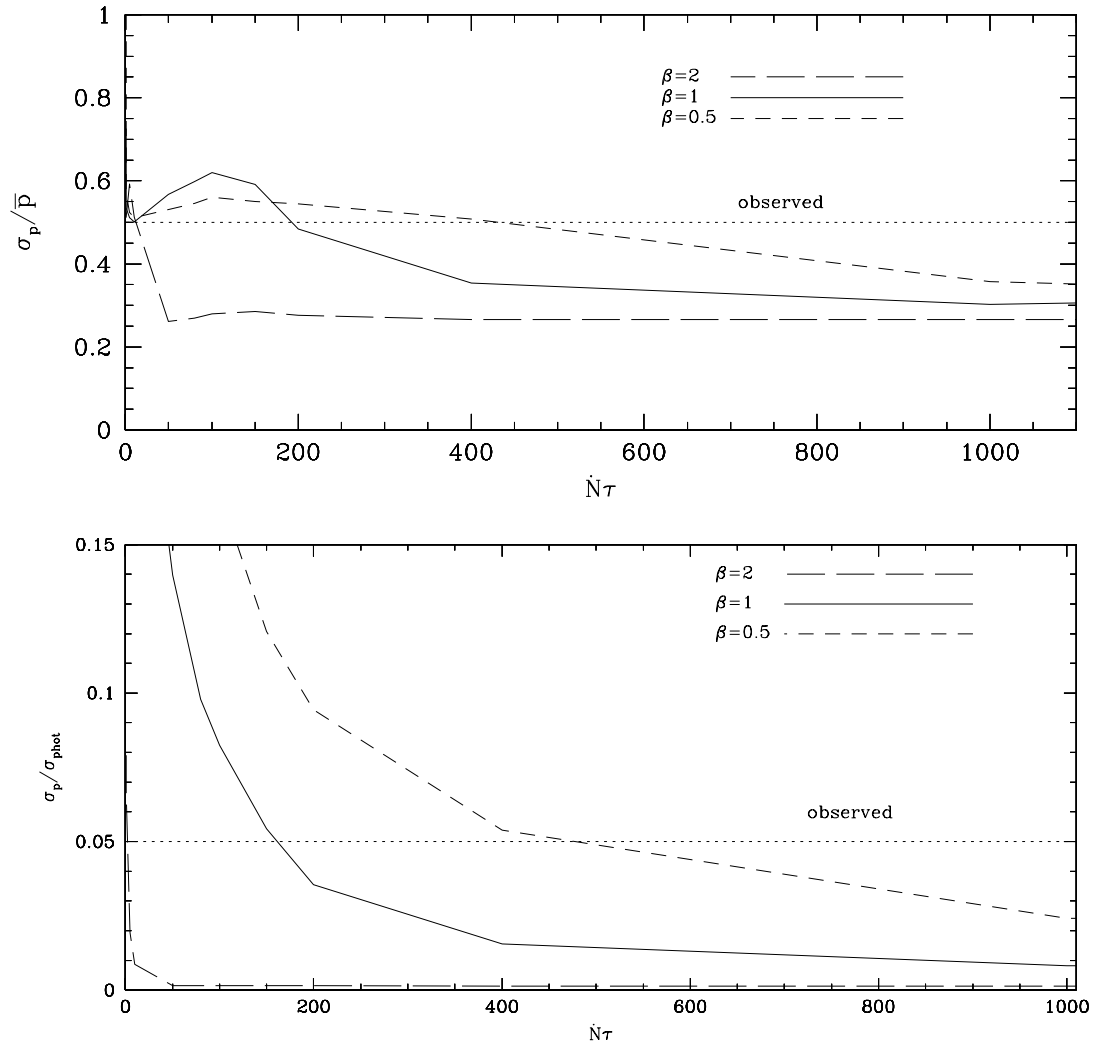


Fig. 4 The upper panel is σ_p/\bar{p} vs \mathcal{N} in various cases of β as denoted in the plot. The lower panel is $\sigma_p/\sigma_{\text{phot}}$ vs \mathcal{N} . The observed are denoted in dotted lines in two panels.

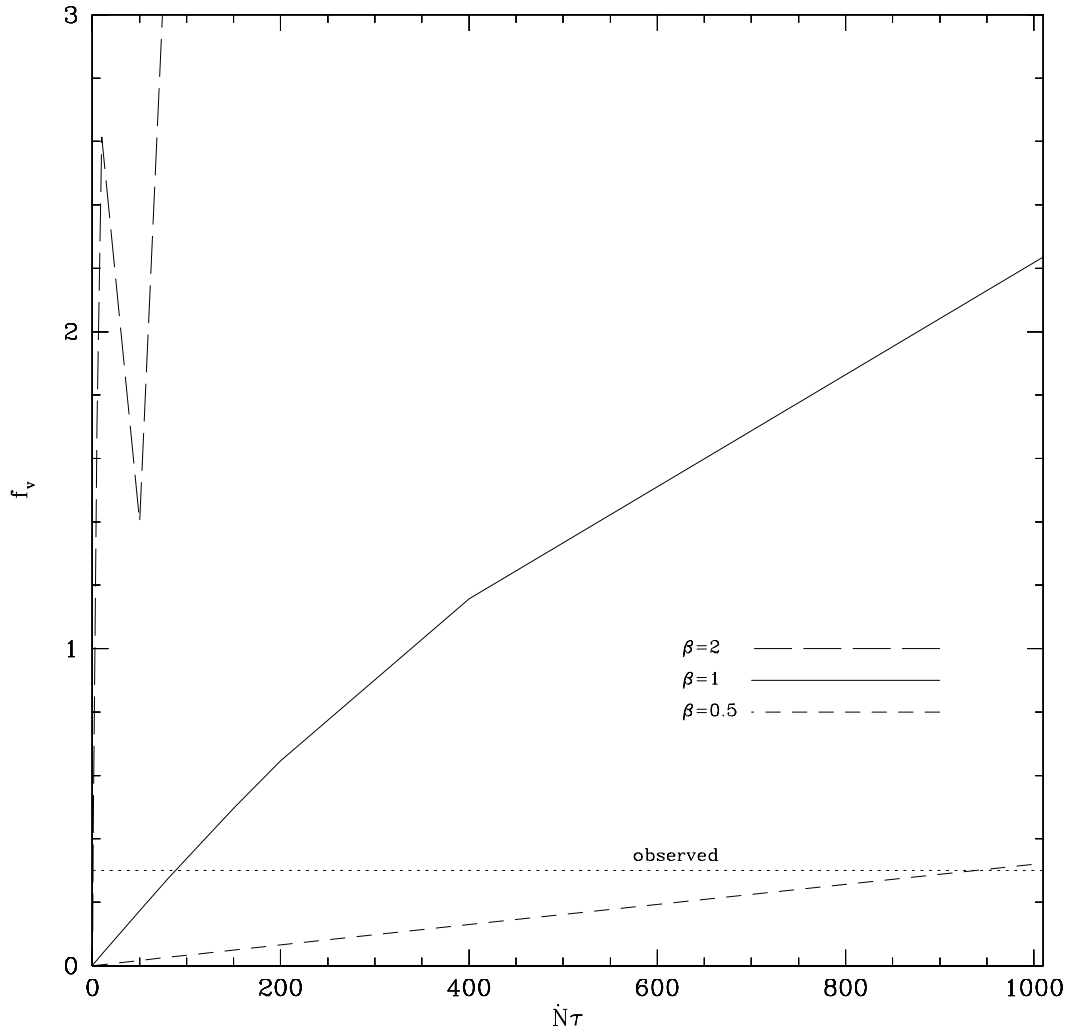


Fig. 5 Volume filling factor f_v vs \mathcal{N} in various cases of β as denoted in the plot.

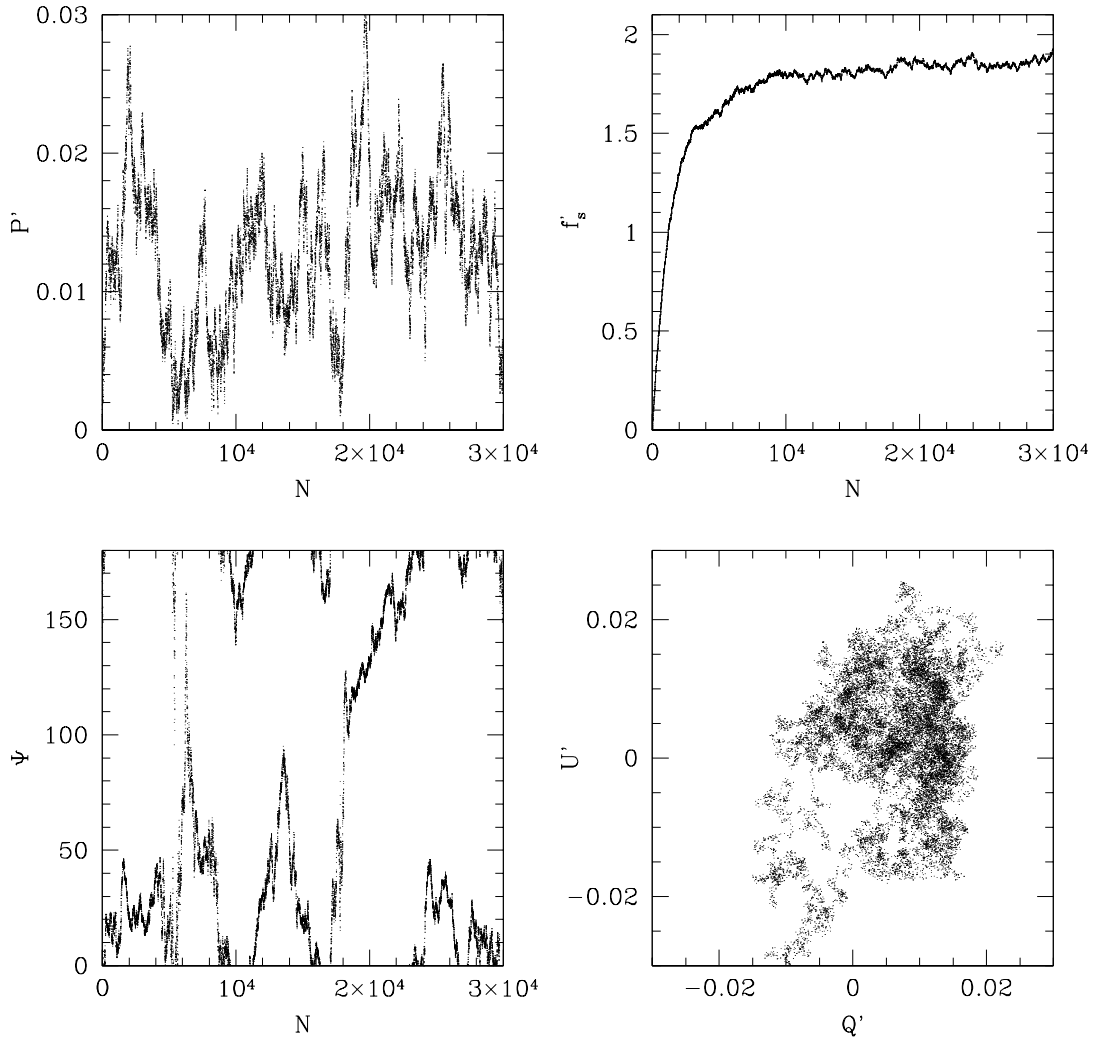


Fig. 6 The figures show respectively, instant by instant, model results vs number N of clumps emitted thus far for the following: upper left panel – polarization $p' = p/p_0$; upper right – scattered light $f'_s = f_s/f_0$; lower left panel – polarization position angle ψ ; lower right panel – $Q' = Q(N)/p_0$ versus $U' = U(N)/p_0$. $\beta = 0.5$ and $\mathcal{N} = 1000$ are applied.

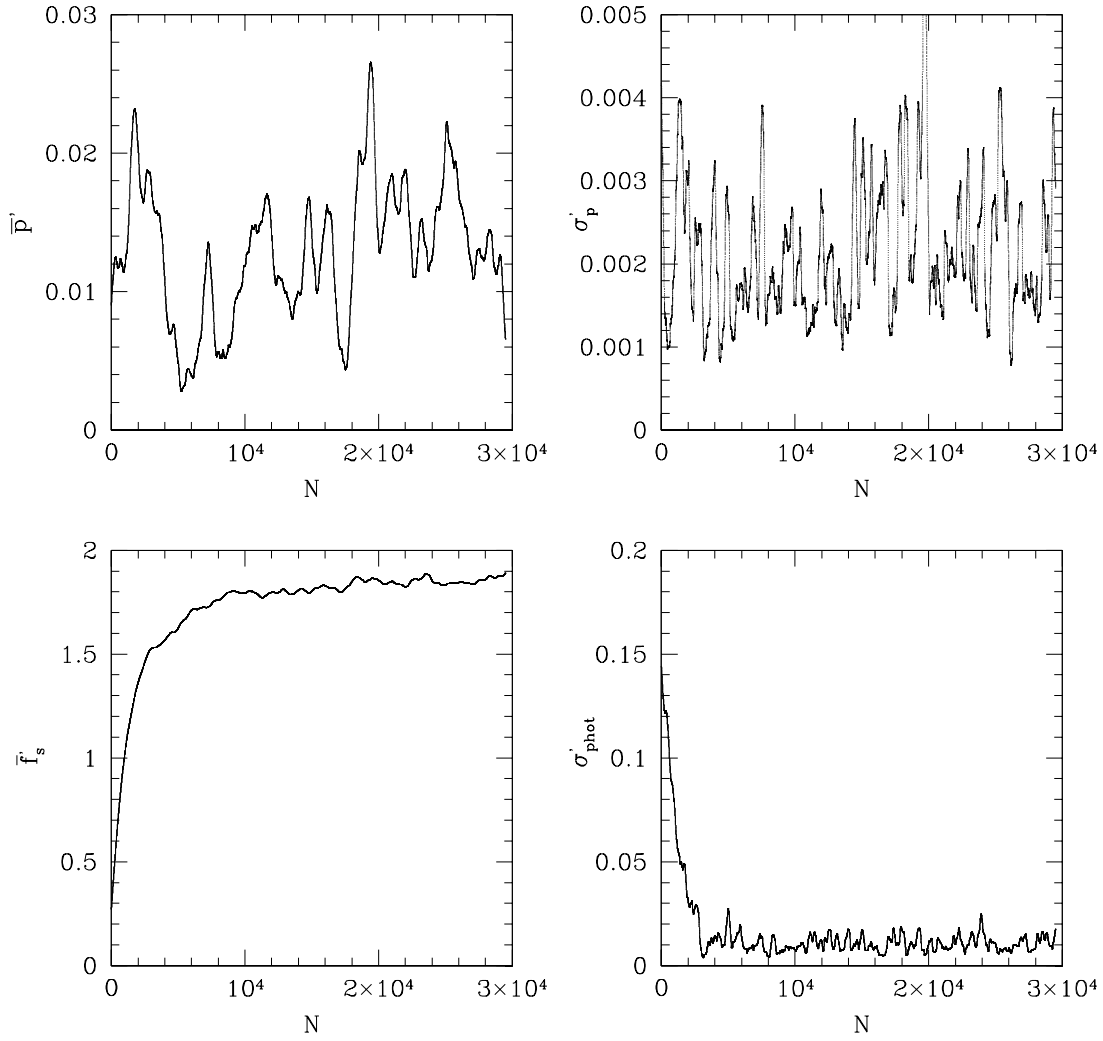


Fig. 7 Based on the same data as Fig. 6, here we show smoothed results versus number of clumps N (increasing with time) for the following observables, with parameters as in Fig. 6: (a) mean polarization $\bar{p}' = \bar{p}/p_0$; (b) variance of polarization $\sigma_p' = \sigma_p/p_0$; (c) mean scattered light fraction $\bar{f}_s' = \bar{f}_s/f_0$; (d) variance of scattered light $\sigma_{\text{phot}}' = \sigma_{\text{phot}}/f_0$.

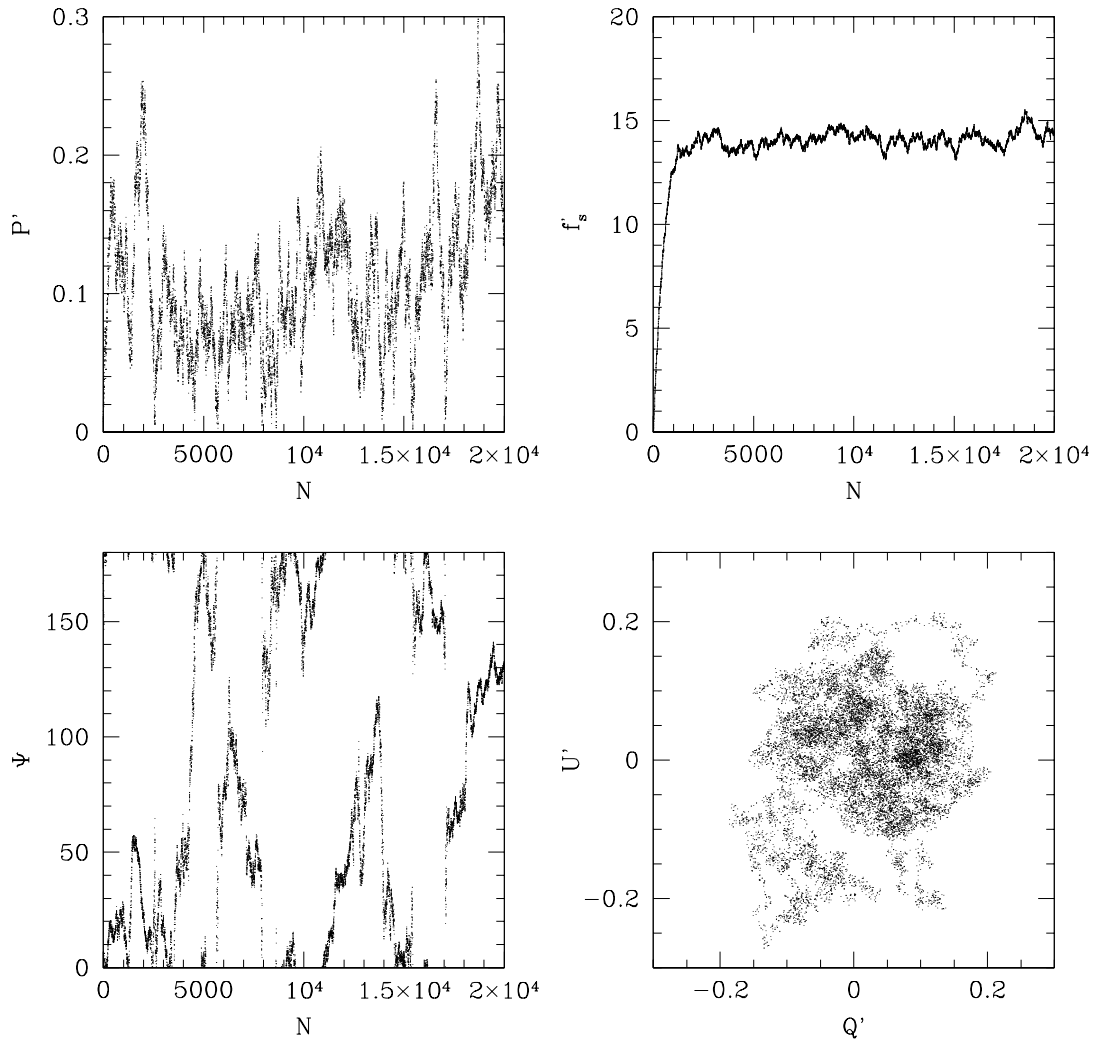


Fig. 8 The figures are similar to Fig. 6, except $\beta = 1$ and $\mathcal{N} = 200$ are applied.

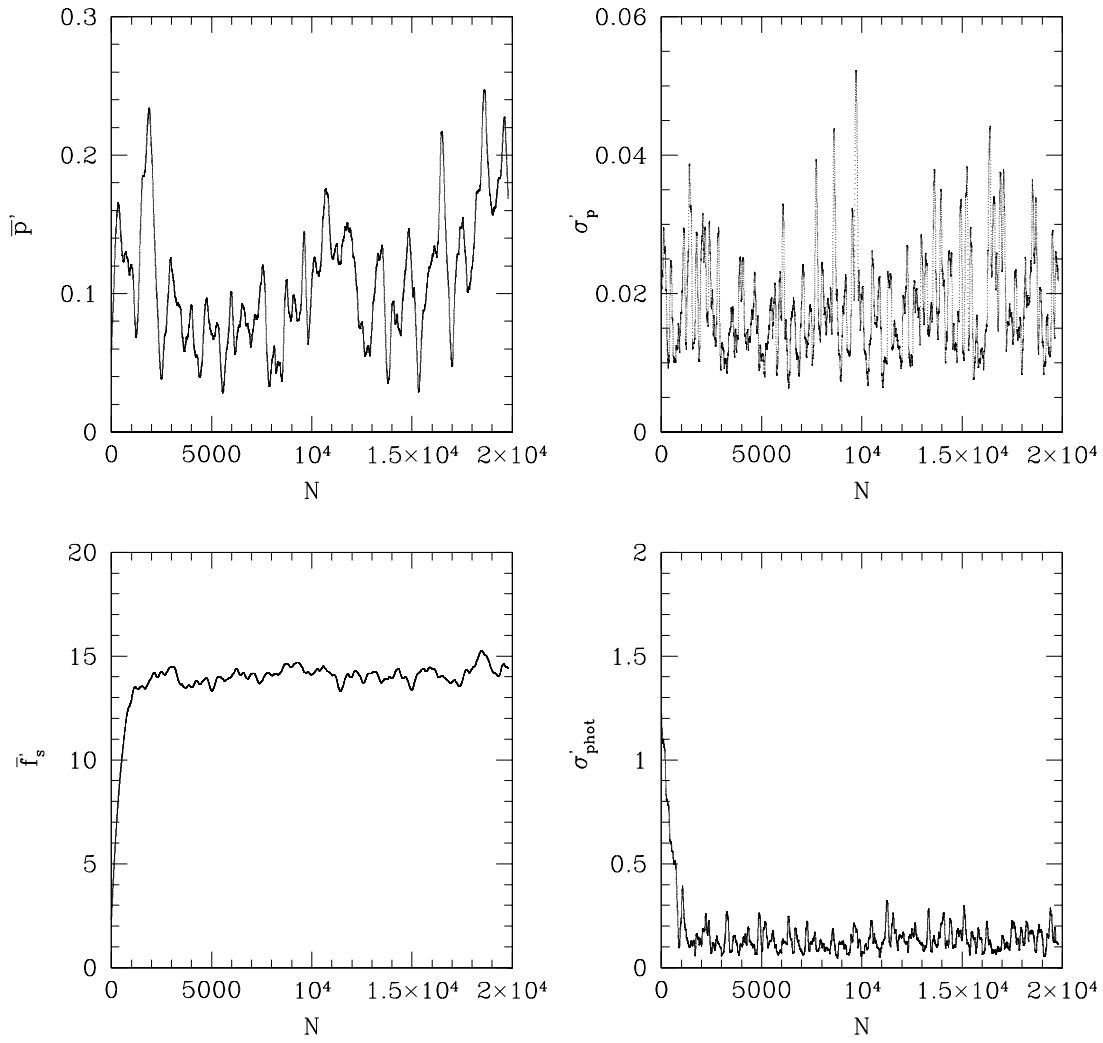


Fig. 9 The figures are similar to Fig. 7, except $\beta = 1$ and $\mathcal{N} = 200$ are applied.

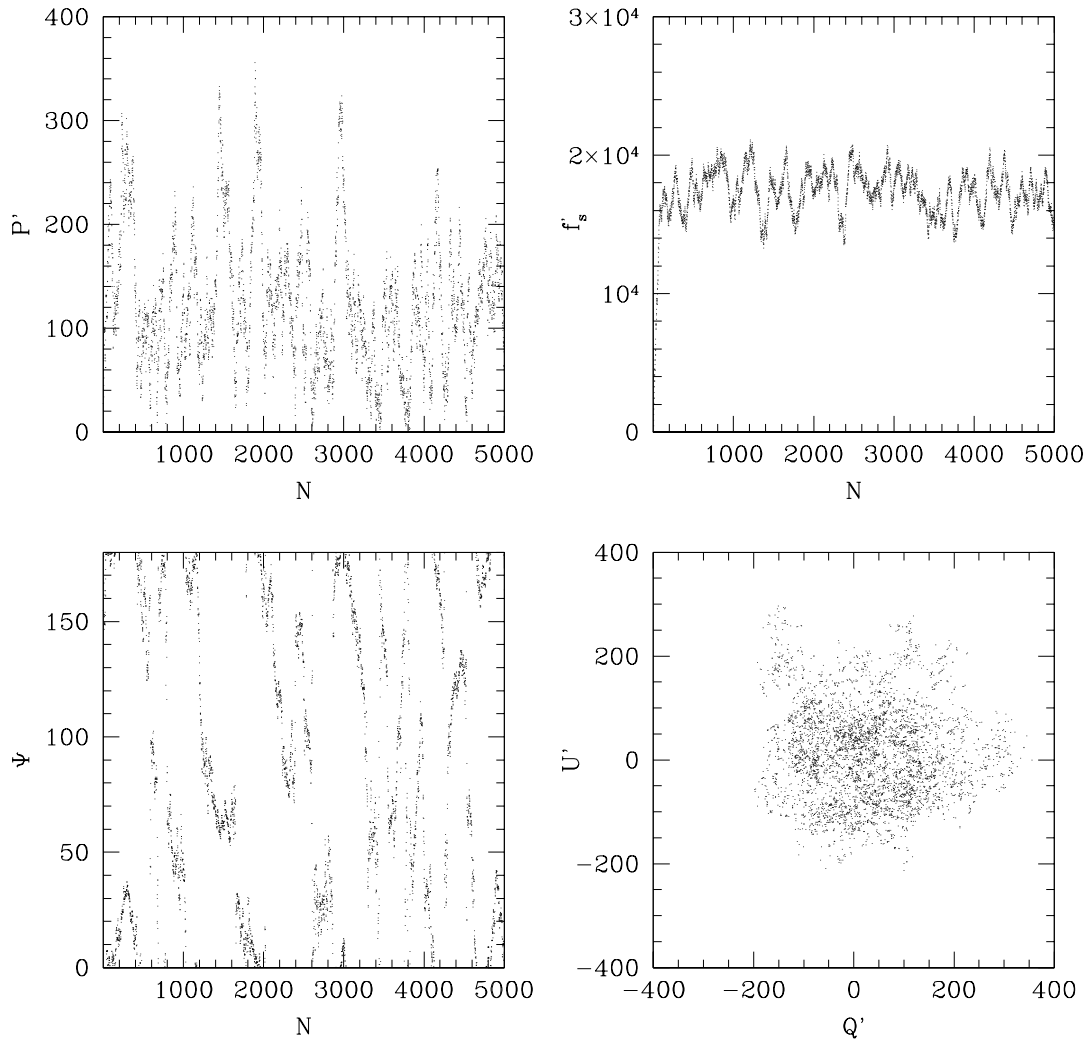


Fig. 10 The figures are similar to Fig. 6, except $\beta = 2$ and $\mathcal{N} = 1$ are applied.

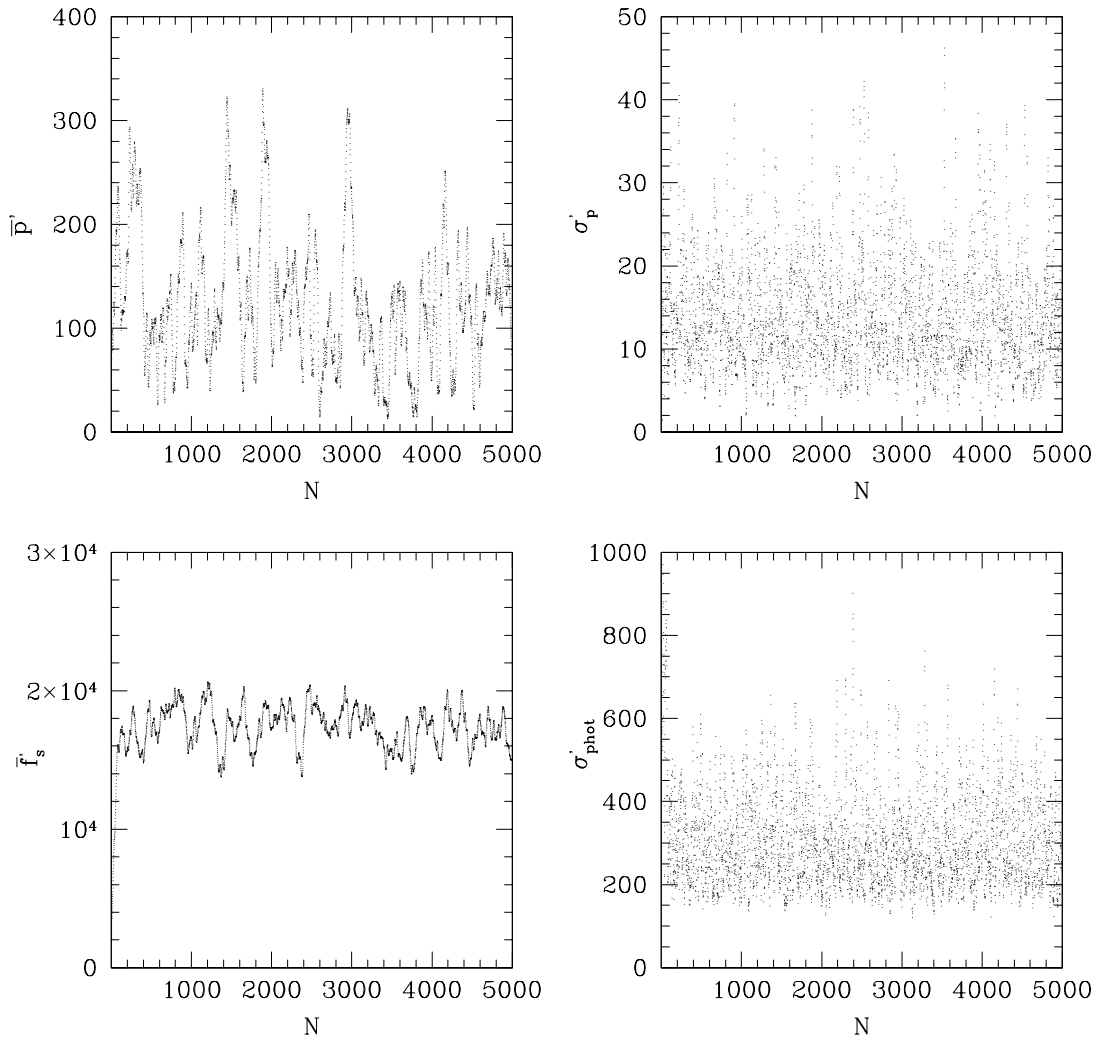


Fig. 11 The resulting figures are similar to Fig. 7, except $\beta = 2$ and $\mathcal{N} = 1$ are applied.

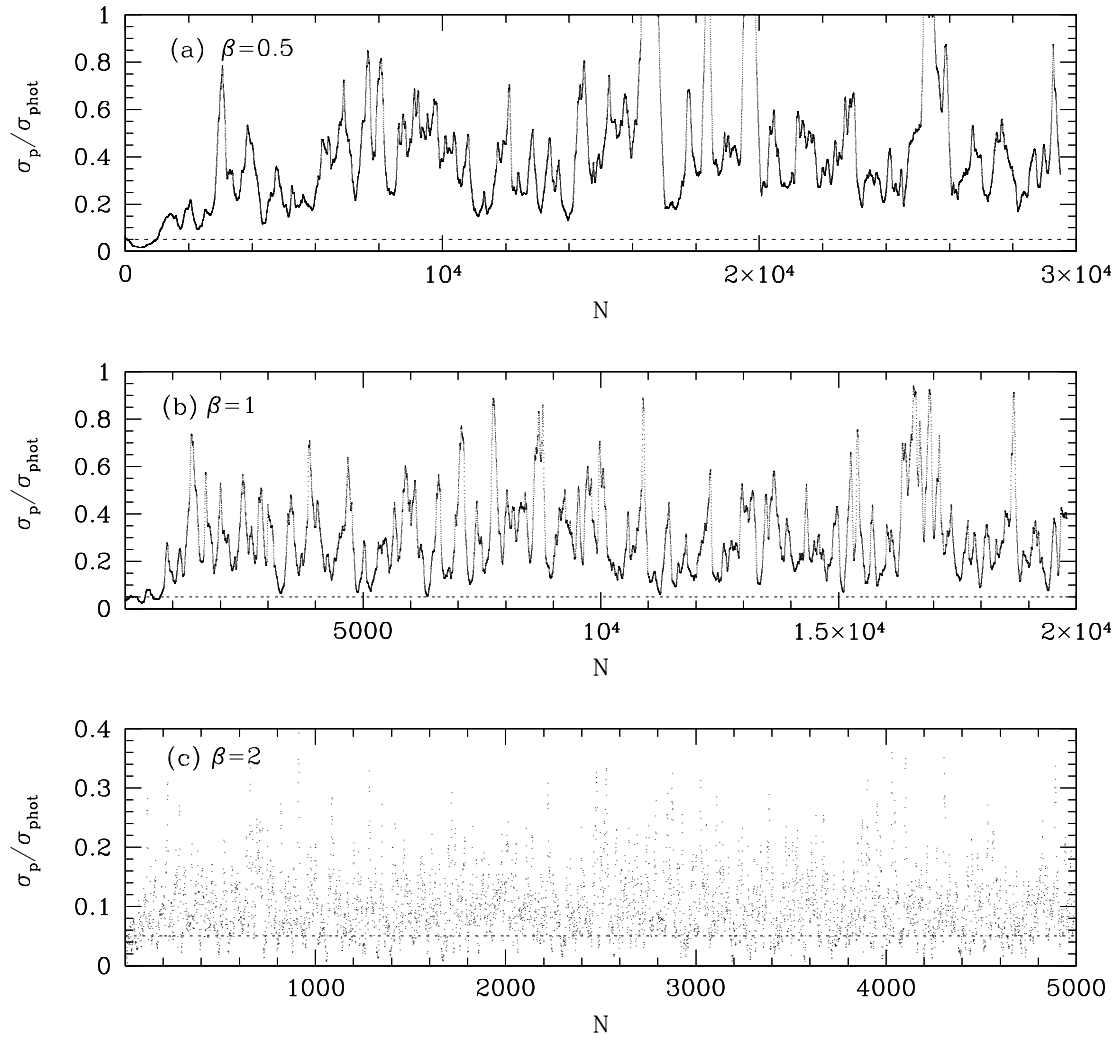


Fig. 12 Ratio ($\mathcal{R} = \sigma_p/\sigma_{\text{phot}}$) of polarimetric to photometric standard deviations vs number of clumps N . The upper panel (a) is for $\beta = 0.5$ and $\mathcal{N} = 1000$. The middle panel (b) is for $\beta = 1$ and $\mathcal{N} = 200$. The lower panel (c) is for $\beta = 2$ and $\mathcal{N} = 1$. The steady mean value \mathcal{R} about 0.05 can be sustainable in case of $\beta = 2$ and $\mathcal{N} = 1$.

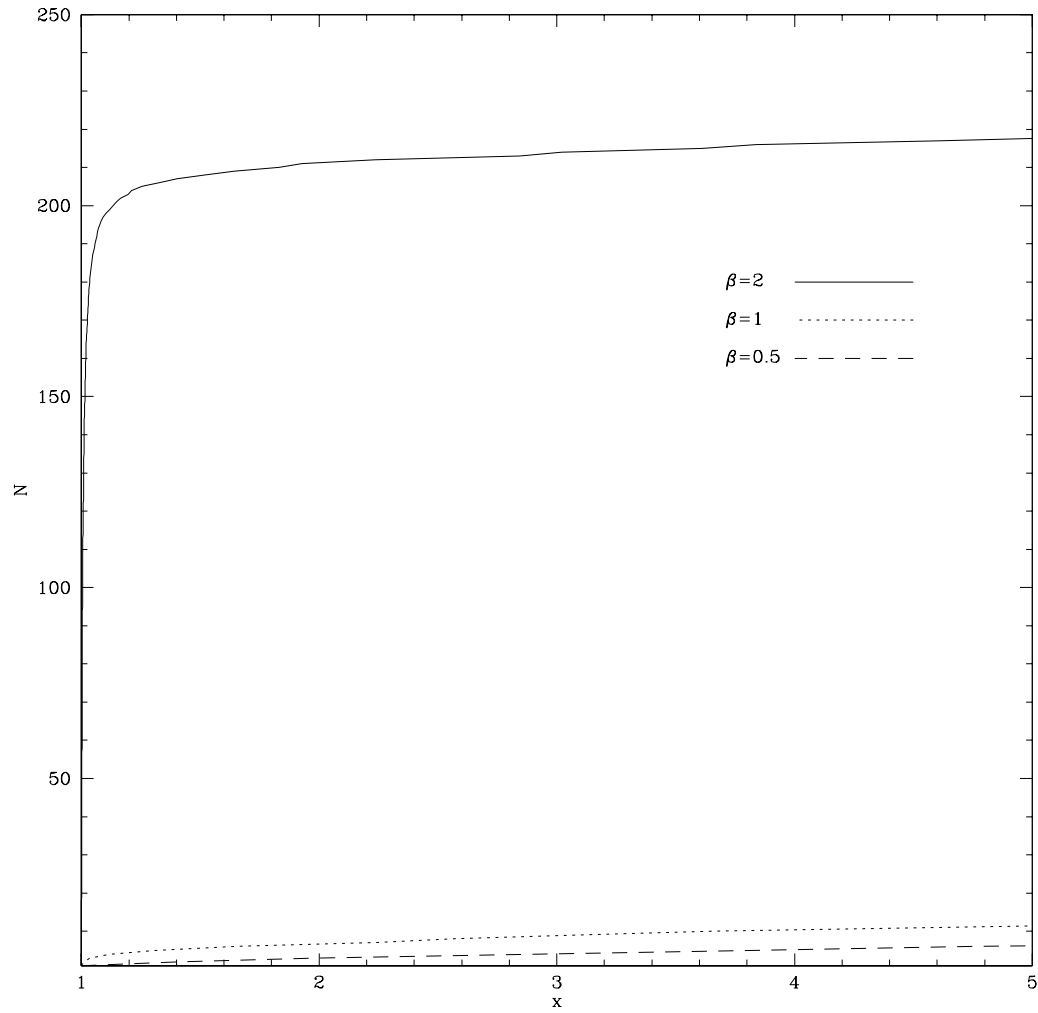


Fig. 13 The number of clumps N vs the radial distance (x) in case of $\mathcal{N} = 1$. The solid line is for $\beta = 2$, the dotted line is for $\beta = 1$, and the dashed line is for $\beta = 0.5$. Due to the “dwelling” time around the star is longer in case of larger β , the number of clumps are more, in comparison with the smaller β case.